Article

Innovative Anodic Treatment to Obtain Stable Metallic Silver Micropatches on TiO$_2$ Nanotubes: Structural, Electrochemical, and Photochemical Properties

Valentina C. Cajiao Checchin, Rodolfo D. Cacciari, Aldo A. Rubert, Marcela Lieblich, Paula Caregnato,* Natalia S. Fagali, and Mónica Fernández Lorenzo de Mele*

Read Online

| ACCESS | | Metrics & More | | Article Recommendations | | SI Supporting Information |

ABSTRACT: Electrochemical modification of the Ti surface to obtain TiO$_2$ nanotubes (NT-Ti) has been proposed to enhance osseointegration in medical applications. However, susceptibility to microbial adhesion, linked to biomaterial-associated infections, and the high TiO$_2$ band gap energy, which allows light absorption almost exclusively in the ultraviolet (UV) region, limit its applications. Modifying the TiO$_2$ semiconductor with metals such as Ag has been suggested both for antimicrobial purposes and for absorbing light in the visible region. The formation of NT-Ti with Ag micropatches (Ag-NT-Ti) is pursued with the objective of enhancing the stability of the deposits and preventing cytotoxic levels of Ag cellular uptake. The innovative process proposed here involves immersing NT-Ti in a AgNO$_3$ solution as the initial step.

Diverging from previously reported electrochemical methods, this process incorporates anodization within the TiO$_2$ oxide formation region instead of cathodic reduction generally employed by other researchers. The final step encompasses an annealing treatment. The treatments result in the *in situ* Ag^{1+} reduction and formation of stable and active micropatches of metallic Ag on the NT-Ti surface. Scanning electron microscopy (SEM), energy-dispersive X-ray spectroscopy (EDS), X-ray photoelectron spectroscopy (XPS), Raman, diffuse reflectance spectroscopy (DRS), wettability assessment, and electrochemical characterizations were conducted to evaluate the modified surfaces. The well-known properties of NT-Ti surfaces were enhanced, leading to improved photocatalytic activity across both visible and UV regions, significant stability against detachment, and controlled release of Ag^{1+} for promising antimicrobial effects.
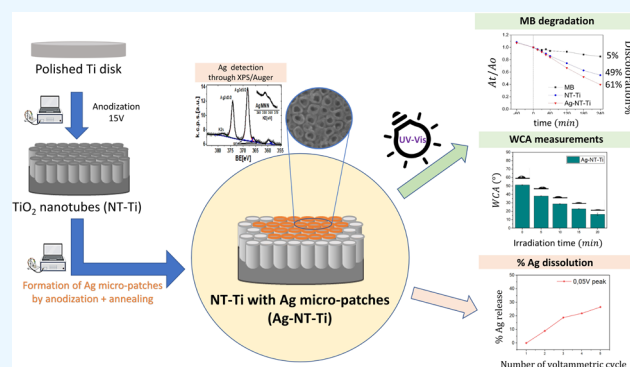
1. INTRODUCTION

Titanium (Ti) is extensively used as a metallic biomaterial for several purposes, including orthopedic and dental implants, due to its outstanding mechanical properties, corrosion resistance, and biocompatibility.[1] It is known that a soft and dense TiO$_2$ film is spontaneously formed on a smooth Ti surface, but this layer is slightly unsuitable for the adhesion of osteoblastic cells, leading to inflammation and loosening of the implant.[2−4] TiO$_2$ nanostructures, such as nanotubes (NT-Ti), have been proposed to enhance the biological response as they exhibit larger specific surface areas capable of improving osteoblast differentiation and promoting substrate tissue interlocking, thereby offering superior biocompatibility.[5,6] Zwilling et al. were the first to report the synthesis of NT-Ti via the electrochemical anodization.[7] Combined methods were also developed to improve NT-Ti efficiency for environmental and industrial purposes.[8,9] Currently, it is known that the chemical composition of NT-Ti and its topographic and photocatalytic properties are strongly dependent on the conditions of anodization and complementary processes.[8,10,11] Despite

remarkable attributes of NT-Ti for medical applications, a significant disadvantage is their susceptibility to microbial adhesion and bacterial biofilm formation,[12,13] one of the major causes of implant failures.[14] Antimicrobial effects can be achieved through the photocatalytic activity of the TiO$_2$ structures. Furthermore, UV irradiation serves as an effective method for removing organics from the surface of NT-Ti, making it a suitable cleaning pretreatment for implants. It also increases the wettability of these surfaces, promoting interaction with cells.[15−17] However, the photocatalytic activity is somewhat limited due to the high band gap energy of TiO$_2$. To overcome this limitation, the modification of TiO$_2$ semi-

conductors with metals such as Ag has been proposed.[18] This not only provides antimicrobial properties of the added metal but also enables absorption of light in the visible region.[19−22] Different methods to load NT-Ti with Ag nanoparticles were proposed in pioneering reports.[23,24] Recently, new procedures for generating Ag-loaded TiO_2 surfaces have been reported,[19,20,24,25] including the deposition of Ag/Ag_2O particles using sol−gel methods, hydro/solvothermal methods, chemical reduction techniques, photodeposition processes, and coprecipitation. However, it has been reported that Ag nanoparticles may induce cell stress and result in the cellular uptake of nanoparticles. These findings emphasize the importance of careful design of Ag-containing structures/deposits to minimize cellular toxicity.[26,27]

To evade the formation and deposition of nanoparticles and their possible cytotoxic effects, an alternative surface modification procedure is proposed here. This process involves immersing NT-Ti in a $AgNO_3$ solution and, unlike previously reported electrochemical methods that include a cathodic reduction step,[28−31] it is followed by anodization at +0.8 V saturated calomel electrode (SCE) within the TiO_2 oxide formation region (Figure 1).
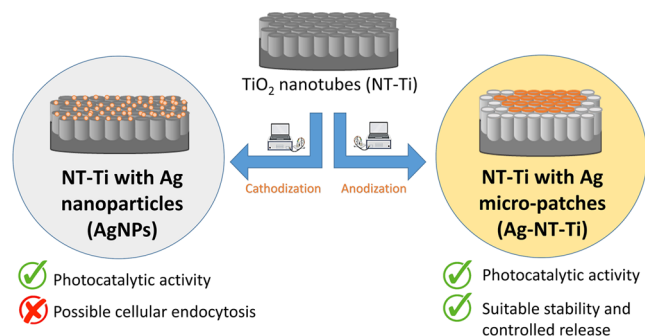

Figure 1. Formation of Ag deposits on the Ti substratum with NT-Ti by cathodic and anodic polarization leading to Ag nanoparticles (Ag-NPs) or Ag micropatches (Ag-NT-Ti).

The treatment, including a final annealing step, led to the *in situ* reduction and formation of stable and active micropatches of metallic Ag on the NT-Ti surface. The resulting surface showed photocatalytic activity in both the UV and visible regions. Also, the patches were gradually released to the aqueous environment with promising antimicrobial activity.

2. EXPERIMENTAL METHODS

2.1. Sample Composition and Pretreatment. Grade 2 titanium (commercially pure, p-Ti) was used in this study (Ti ≥ 99.3%, C 0.011%, N 0.022%, O 0.14%, Fe 0.2%, H 0.002%). The cp-Ti discs with a diameter of 9 mm and 1 mm thickness were obtained from NMM Machinery Manufacturing Co. Ltd. (Guangdong, China). The disks underwent mechanical polishing using SiC sandpaper with various grit sizes, including P320, P400, P600, P1000, P1500, and P2500. Finally, a mirror finish was achieved using 1 μm grain alumina.

2.2. Nanotube Synthesis and Ag Patch Formation. Mirror-polished p-Ti discs were subjected to anodization at 15 V in two cycles, each lasting for 2 h. The anodization was carried out using a solution consisting of 0.3 wt % HF (Sigma-Aldrich), 1 M H_3PO_4 (Cicarelli), and bidistilled water and employing a high-density polyethylene cell with a two-electrode arrangement. A graphite bar served as the cathode, while the p-Ti disk

functioned as the anode. The cell was magnetically stirred at room temperature. For the anodization treatment, a DC power source (ENDURO 300 V power supply, Labnet International, Inc.) was employed. The process was monitored by performing current vs. time records following established procedures.[32−34] The samples were immersed in KCl to measure OCP values (step 1), and afterward, they were submerged in a 1.5 mM $AgNO_3$ (Ag-NT-Ti) or KNO_3 solution (NT-Ti) and subjected to anodization at +0.8 V for 15 min (step 2) and finally annealed at 400 °C (step 3) (refer to Figure 1S in the Supporting Information for current vs time records). The discs were sequentially rinsed with absolute ethyl alcohol (Cicarelli, 99.5%) and distilled water. Finally, they were stored at room temperature.

2.3. Physicochemical Characterization. *2.3.1. Open-Circuit Potential (OCP) Measurements and Cyclic Voltammetry (CV).* Prior to the CV electrochemical test, the OCP was measured during a 5 min stabilization period in 1.5 mM KCl, (Figure 2S). Reproducibility was ensured by repeating each experiment at least three times.

The electrochemical measurements were made in a three-electrode undivided glass cell. The annealed NT-Ti and Ag-NT-Ti and p-Ti control discs (0.64 cm^2) were used as working electrodes. A platinum foil and a SCE were employed as the counter and reference electrodes, respectively. During the CV assays, the electrode potential was successively cycled (five cycles) in the potential range of −1.0 to +1.0 V in alkaline medium (0.01 M NaOH + 0.1 M Na_2SO_4) at a scan rate of 10 mV/s, to characterize the samples.[35] All measurements were performed at room temperature.

2.3.2. Scanning Electron Microscopy (SEM) and Energy-Dispersive X-ray Spectroscopy (EDS) Analysis. The surface features of the samples were observed using scanning electron microscopy (SEM) (HITACHI S4800 microscope, Hitachi High-Tech Corporation, Tokyo, Japan), coupled with energy-dispersive X-ray spectroscopy (EDS) for surface elemental composition analysis. SEM images were captured at magnifications of 5000×, 30,000×, and 100,000×, using secondary electrons (SE) and backscattered electrons (BSE) to investigate topography and the distribution of various elements, respectively.

2.3.3. Calculation of Nanotube Length through Indentation. The indentation test (Matsuzawa seiki Co., Ltd.) was used to determine the length of nanotubes. A force of 1 kg on the surface of the sample with a 136° diamond pyramid indenter was applied. The indentation depth (h) was calculated to estimate the length of the nanotube layer (see the Supporting Information for more details).

2.3.4. Raman Spectroscopy. Raman spectroscopy measurements of the NT-Ti and Ag-NT-Ti samples were performed using a HORIBA JobinYvon T64000 Raman microspectrometer (Tri-Grate Raman Spectrometer). The Raman spectrum was obtained by employing an argon laser beam with a wavelength of 512 nm and an output power of 500 mW. The instrument was coupled with a confocal microscope and CCD detector.

2.3.5. X-ray Photoelectron Spectroscopy (XPS). X-ray photoelectron spectroscopy (XPS) measurements were carried out using a nonmonochromatic Mg Kα source (XR50, Specs GmbH) and a hemispherical electron energy analyzer (PHOIBOS 100, Specs GmbH) operating in fixed transmission analysis mode with pass energies of 40 and 10 eV. A two-point calibration of the energy scale was performed using gold (Au 4f$_{7/2}$, binding energy BE = 84.00 eV) and copper (Cu 2p$_{3/2}$, BE =

932.67 eV) samples cleaned with a sputtering ion gun. The analysis was carried out at a takeoff angle of 90°, and adventitious carbon (component C 1s at 284.8 eV) was used as a charging reference, when necessary. The pressure during the measurements was typically in the range of 10^{-9} mbar. XPS data were analyzed using CASA-xps v2.2.99 software, employing a Shirley-type background line. Quantification analysis based on peak areas and the relative sensitivity factor was employed. The Auger parameter (AP) was calculated to assess the chemical modification of the surface by Ag species, independently of the static charge of the substrate.[36]

The quantification method used utilizes the atomic percentage (atom %), considering all the signals detected for all the elements. The analysis is typically performed at a depth equivalent to three times the electron attenuation length (AL).[37] The quantification method assumes no geometry preference by analytes. The area analyzed on the sample was a 5 mm-diameter circle, covering the middle portion of the sample and excluding signals from the sample holder.

2.3.6. Diffuse Reflectance Spectroscopy (DRS). DRS was performed using a PG Instruments T90+ UV−vis spectrophotometer equipped with an integrating sphere. DRS spectra were recorded during the analysis.

2.3.7. Photocatalytic Assays. Photocatalytic assays were conducted in a 3.5 mL fluorescence cell at a temperature of 25 °C, in ambient air, and with continuous magnetic stirring for a period of 3 h. The methylene blue (MB) solution was prepared by adjusting the absorbance to 0.5 at the maximum wavelength of 664 nm. The NT-Ti and Ag-NT-Ti samples were immersed in the cell containing the MB solution and kept in the dark for 1 h under magnetic stirring to achieve an adsorption/desorption equilibrium before irradiation.

To evaluate the photocatalytic capabilities of NT-Ti and Ag-NT-Ti, a Rayonet RPR-100 photochemical reactor (Southern New England Ultraviolet Company) was employed. The reactor was equipped with eight interchangeable lamps emitting at a wavelength of 350 nm for UV illumination. For visible light assays, an optical arrangement comprising two 430 nm light-emitting diodes (LEDs) served as the irradiation source. The photon flux reaching the reaction cell was determined by using actinometrical measurements, resulting in a value of 0.0065 J/s for the UV lamps and 0.0016 J/s for the visible light arrangement.

The quantification of MB at different irradiation times was made by using a UV−vis spectrophotometer (PG Instruments T90+). The absorbance at 664 nm at time t (A_t) was compared with the absorbance at $t = 0$ (A_0) to calculate the degree of discoloration (discoloration %) according to eq 1

$$\text{discoloration \%} = \left(\frac{(A_0 - A_t)}{A_0} \right) \times 100 \tag{1}$$

In control experiments, the evolution of the MB concentration in aqueous solution was monitored under irradiation (without NT-Ti) and without irradiation (but with NT-Ti). The results indicated neither significant adsorption of the dye on the material nor substantial direct photolysis of MB with UV and Vis light during the experiment duration in comparison to the initial concentration of MB.

2.3.8. Contact Angle Measurements. Contact angle measurements were performed to assess the water−air interface contact angles (WCA) on the surfaces of p-Ti, NT-Ti, and Ag-NT-Ti. Additionally, WCA measurements were conducted

during UV irradiation on the Ag-NT-Ti sample after various periods (within the 0−20 min range). A Ramé-Hart Instrument Co. Mod 290-U1 was used with a droplet of 1 μL of distilled water for the measurements. Three replicates of each sample were analyzed, with ten measurements taken for each replicate. The average value was calculated by using the DROP Image Advanced program.

3. RESULTS AND DISCUSSION

3.1. Scanning Electron Microscopy (SEM) Coupled to Energy-Dispersive X-ray Spectroscopy (EDS). Figure 2A
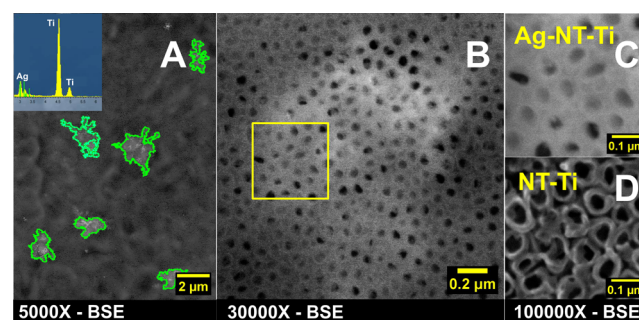

Figure 2. Microscopic evaluation of surface features of NT-Ti and Ag-NT-Ti and surface elemental composition. (A) Scanning electron microscopy (SEM) image with backscattered electrons (BSE) at 5000× magnification of the Ag-NT-Ti surface. Ag patches as *ca.* 2 μm patches are outlined with green lines for clarity. (Inset) Representative energy-dispersive X-ray spectroscopy (EDS) analysis was performed on a Ag patch zone. (B) SEM image with BSE at 30,000× magnification, revealing a Ag micropatch that partially or completely covered some NT openings. (C) Detail of B (yellow square) at 100,000× magnification. (D) SEM image at 100,000× magnification of the NT-Ti sample.

illustrates the configuration and distribution of heavy atom patches on a Ag-NT-Ti sample as bright spots detected through the BSE mode. It is evident that there exist irregularly shaped patches, which are *ca.* 2 μm in length. The average spot area was computed to be 1.4 ± 0.7 μm². EDS analysis (Figure 2A inset) conducted on a patch confirmed that these heavy atoms correspond to Ag. Further magnifications reveal that Ag micropatches partially or completely cover the openings of the nanotubes (Figure 2B,C).

In Figure 2D, the nanotubes developed on the Ti surface exhibit an average outer diameter of 96 ± 15 nm. The average length of the nanotubes was estimated through indentation measurements to be *ca.* 9.6 μm (see Figure 3S for detailed information).

The size of the patches is an important parameter to consider, since it affects different processes. It is well known that the cytotoxicity of Ag nanoparticles (AgNPs) can be mediated by both ionic and particle-mediated mechanisms, but the sensitivity of several types of cells depends on the characteristics of AgNPs/Ag^{1+} suspensions. Besides, cytotoxicity of AgNPs is also linked with the phagocytic ability of each type of cells, which allows them to internalize particles. These particles can later release ions, triggering several ways of cell damage, including enzyme inactivation, oxidative stress leading to apoptosis, or lipid peroxidation resulting in necrosis.[38,39] As previously reported,[40] AgNPs (50 nm) demonstrated strong cytotoxic effects on primary osteoblasts and osteoclasts, while weak cytotoxic effects were observed for Ag microparticles (3 μm). Thus, the
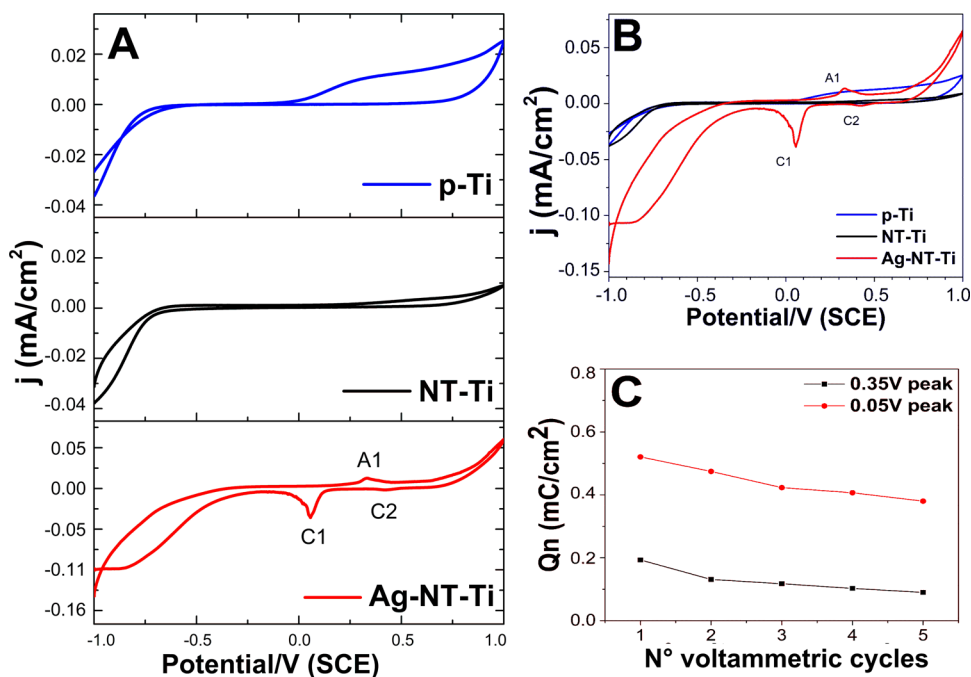
Figure 3. Cyclic voltammetry. (A) Cyclic voltammograms performed at 10 mV/s in alkaline medium with p-Ti, NT-Ti, and Ag-NT-Ti (first cycle). (B) Comparison of the three voltammograms. A1 (Ag oxidation) and C1 and C2 (Ag reduction) current peaks. (C) Decrease in charge vs. number of VC cycles for peaks A1 (0.35 V) and C1 (0.05 V).

cytotoxicity of these cells is primarily mediated by a particle size-dependent release of Ag^{1+}. In the present work, we developed a procedure to obtain micropatches of Ag^0 on NT-Ti with the aim of avoiding the nanoparticle endocytosis[26,27] and controlling Ag^{1+} release, since in the case of nanoparticles, it is exacerbated due to their elevated surface/volume ratio. Additionally, sustained Ag^{1+} release over time that can help prevent bacterial attachment onto the implant surface and eliminate bacteria that have successfully adhered is also guaranteed.

According to recent findings, the combination of micro- and nanostructures, such as the nanotubes with Ag patches on the surface presented here, may enhance cell adhesion. Zheng et al.[41] compared the adhesion of cells to micro/nanotopography with that of smooth topography and irregular microscale topography surfaces to investigate the mechanisms involved in cell−surface interactions. They found that the formation of mature focal adhesions was significantly enhanced in samples with hierarchical micro/nanotopography.[42] Therefore, the combination of micro- and nanostructuring could potentially provide an additional advantage in the osseointegration process, making it worthwhile to gain further insights through more specific assays.

3.2. Electrochemical Measurements. *3.2.1. OCP Measurements.* OCP measurements for NT-Ti in a KCl solution (step 1) revealed a negative potential value of −133.1 mV, aligning with previously documented data.[43] Subsequently, NT-Ti samples were immersed in $AgNO_3$ (from now on Ag-NT-Ti) or KNO_3, followed by an anodizing process at +0.8 V (step 2). Afterward, OCP records were then obtained in a KCl solution over a 5 min period. The final stable potential values were +260.3 mV for Ag-NT-Ti and +92.6 mV for NT-Ti (refer to Figure 2S in the Supporting Information). These values suggest distinct interactions between the electrode surfaces and surrounding liquid environments. The substantial shift in the potential value toward the anodic direction for Ag-NT-Ti (from

−133.1 mV (step 1) to +260.3 mV (step 2)) can be attributed to the formation of heterojunctions, which involve the joining of semiconductors with different properties.[44] It has been suggested that the Ag/TiO_2 and Ag_2O/TiO_2 systems may reduce the charge carrier recombination rate at the TiO_2 surface and contribute to an increase in the OCP of the metal. This effect is likely due to the higher built-in potential resulting from the heterostructure's higher band offset.[45]

3.2.2. Cyclic Voltammetry (CV). To confirm the presence and stability of Ag patches, CV in a wide potential range (−1.0 to +1.0 V) was performed on p-Ti, NT-Ti, and Ag-NT-Ti samples. Figure 3A shows CV curves recorded for the different samples during the first cycle in alkaline medium. In the record of the p-Ti control (blue line), an anodic contribution at potentials higher than 0.0 V, which is associated with TiO_2 formation, is observed. According to the reported data,[33,46] this oxide is not reduced during the cathodic scan, indicating its high stability.

When the annealed NT-Ti was used (Figure 3A black line), a lower anodic current contribution, compared with that of p-Ti, indicates minimal new TiO_2 formation. Thus, the annealing process leads to the formation of a very stable layer of nanostructured oxide (NT-Ti) in agreement with previous results.[32]

In the case of Ag-NT-Ti, CV records (Figure 3A red line) showed a peak at *ca.* 0.35 V (A1 peak), revealing the presence of Ag species on the surface, consistent with EDS data, XPS and AP (see next sections), and previous reports.[34,47] Also, an anodic current contribution at higher potentials was detected near the +1 V limit. Considering that the anodic scan was initiated at −1.0 V and, consequently, all Ag species present on the metal have been reduced at this potential, the anodic current contributions can be attributed to the oxidation of Ag^0 to $Ag_2O/Ag(OH)$ and eventually to AgO at more anodic potentials. Simultaneously, with the formation of Ag_2O, partial Ag dissolution occurs and $Ag(OH)_2$ may be formed.[34] During
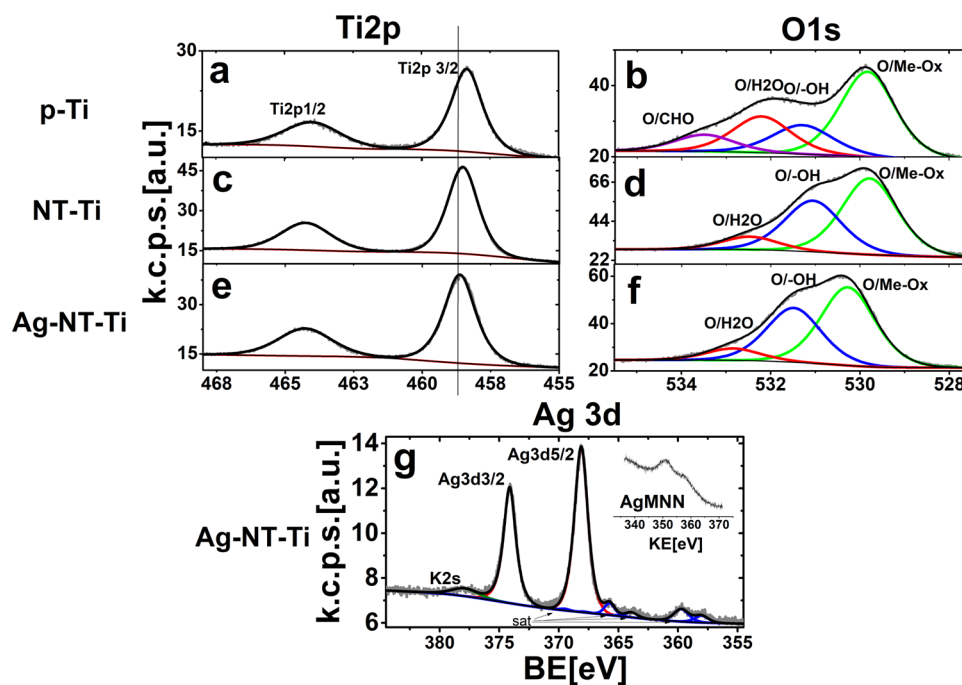
Figure 4. XPS analysis. XP data fitting components for Ti 2p (a, c, e) and O 1s (b, d, f) for p-Ti, NT-Ti, and Ag-NT-Ti substrates, respectively. (g) Representative fitting region of the XP data for the Ag 3d and Auger signal (AgMNN) (inset) for Ag-NT-Ti. Nonmonochromatic source satellites and traces of K 2s from the process obtained with Ag loading are shown. The vertical line in (a), (c), and (e) is an eye guide for BE shift on the Ti 2p signal.

the reverse scan, a small cathodic charge at 0.40 V (C2 peak) and a complex cathodic peak close to 0.05 V (C1 peak) were detected in agreement with previously reported data,[47] which can be associated with the reduction of Ag^{2+} and Ag^{1+} species to Ag^0, respectively.

Additionally, at potentials of more cathodic than −0.5 V, remarkably high negative currents were recorded with the Ag-NT-Ti sample. The cathodic reaction is enhanced in relation to the control due to the probable presence of Ag-TiO_2 heterojunctions that may function as catalysts. Furthermore, it has been suggested that oxygen may be trapped in the Ag-containing nanostructured surface (such as Ag-NT-Ti) at anodic potentials (near the anodic potential limit) and may be reduced close to the cathodic limit of the scan, where a plateau is depicted in the −0.8 V region due to diffusion resistance for oxygen species. The source of oxygen may be traces of air dissolved in the electrolyte or from the oxygen evolution reaction occurring at the anodic potential limit.[48,49] Voltammograms of the first cycle for p-Ti, NT-Ti, and Ag-NT-Ti are shown together in Figure 3B for comparison.

As previously mentioned, peak A1 is related to the oxidation of Ag° species to Ag^{1+} species. Most of these species are reduced in C1.[50,51] However, some of Ag^{1+} may be (i) further oxidized to Ag^{2+} species and then reduced in the C2 potential region to Ag^{1+} or (ii) become soluble Ag species that do not return to the electrode surface. Figure 3C displays the gradual reduction in the charge of peaks A1 and C1 over the course of five voltamperometric cycles. The cycling sequence demonstrates that the electrochemical characteristics of Ag patches are stable since the decrease in charge and current density of the cathodic peak related to the release of Ag^{1+} species occurs gradually, without abrupt current shifts, characteristics of metal detachments.[52] No abrupt shifts in OCP values related to metal detachments were recorded during the assays.[53]

3.3. XPS Measurements. Figure 4a−f shows the Ti 2p and O 1s regions for p-Ti (a and b), NT-Ti (c and d), and Ag-NT-Ti (e and f) samples. The BE found for Ti 2p was 458.33, 458.55 and 458.59 eV (Ti $2p_{3/2}$) and 463.90, 464.29, and 464.30 (Ti $2p_{1/2}$) for p-Ti, NT-Ti, and for Ag-NT-Ti, respectively. These values do not differ from those reported for the native TiO_2 formed on the Ti substrate and from those informed for the anatase.[54,55] However, NT-Ti and Ag-NT-Ti show a slight shift to higher BE with respect to polished samples, and this may indicate that the Ti−O environments in polished samples and samples with NT-Ti are slightly different. Chae et al. also observed, in the case of TiO_2 nanoparticles, significant BE changes for Ti $2p_{3/2}$ that were interpreted as interactions in oxygen environments, leading to positive polarizability of Ti−O bonding. The authors anticipated an increase in energy conversion efficiency for modified TiO_2.[56]

Figure 4b,d,f shows XP lines for O 1s regions for p-Ti, NT-Ti, and Ag-NT-Ti, respectively. These regions depict components at 529.79 to 530.31 eV typical of metal oxides (named O/MeO_x), 531.00 to 531.55 eV corresponding to hydroxylated species (O/−OH) or O/X−O, where X may be P, N, etc., and 532.15 to 532.88 assigned to the oxygen signal from physisorbed water (O/H_2O). The p-Ti sample has another O 1s component located close to 533.54 eV and this was assigned to oxygen compounds in organic components (O/CHO).[57,58]

The O/CHO and most of the O/H_2O signals were removed when the Ti surface was modified to give NT-Ti and Ag-NT-Ti. In addition, for samples with NT (Ag-NT-Ti and NT-Ti), a difference in the O/Me−O_x and O/OH signal ratios can be observed, with a higher O/OH ratio than that of the p-Ti samples. These data agree with a possible increase in specific surface area (detected by atomic force microscopy in previous work), which is consistent with NT formation.[32] After the treatments to obtain Ag-NT-Ti, the ratio of the O/Me−O_x and the O/OH signals does not change appreciably with respect to
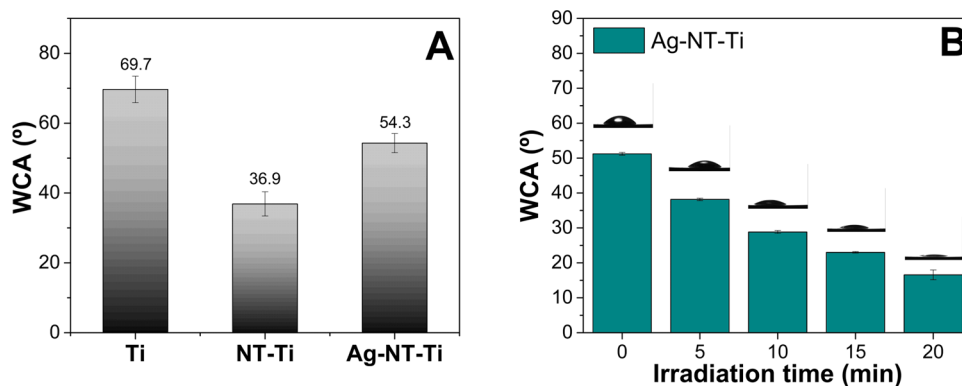
Figure 5. Wettability measurements. WCA measurements of (A) p-Ti, NT-Ti, and Ag-NT-Ti samples and (B) Ag-NT-Ti after different UV irradiation periods.

NT-Ti. However, the signal shifts toward a higher BE as can be seen in Figure 4f. Since there is a large number of reported species assigned to the O 1s, no species were reassigned here. It is possible that structural changes or defects at the border of the NT may alter the environment of the oxygen species. Although the difference between Ag-NT-Ti and NT-Ti samples is 3% Ag (3% Ag = Ag atomic average surface loading (%) and Ag/(Ag + Ti) = 0.20 atomic relationship), the interaction of Ag with the NT is significant. This suggests that the Ag loading on the Ag-NT-Ti surface is located at a shallow depth (Ag metallic micropatches on Ag-NT-Ti as shown in the micrographs) or in regions that do not significantly attenuate the photoelectron signals.

In agreement with the EDS data and CV results, XPS shows photoelectron signals of Ag 3d in Ag-NT-Ti samples (Figure 4g). In relation to describing the oxidation states of metals, there is a wide agreement in considering the AP more suitable than BE of Ag $3d_{5/2}$.[35,59−61] In Figure 4g inset, AgMNN regions were reported. Combined photoelectron data and Auger signals gave an AP value (726.12 eV) close to that reported for metallic Ag (726.09),[57] confirming the presence of Ag^0 as the main species.

3.4. Contact Angle Measurements. Figure 5A shows the contact angle values in the order Ti > Ag-NT-Ti > NT-Ti. As described by Ryan et al.,[62] contact angle values exhibit variability when not corrected for roughness effects. Thus, when a water droplet fully wets a rough surface, the contact angle can decrease on a hydrophilic surface and increase on a hydrophobic surface. However, in cases where a liquid droplet does not entirely wet the rough surface, there are pockets of air between the droplet and the substrate that leads to heterogeneous wettability. In this study, the presence of nanotubes (NT-Ti and Ag-NT-Ti) indicated a more hydrophilic behavior compared to smooth p-Ti, suggesting higher wettability on these rough surfaces. However, due to partial coverage of some nanotube openings by Ag patches, the contact angle for Ag-NT-Ti was found to be higher than that of NT-Ti. This increase in the contact angle can be attributed to the presence of the Ag patches where a direct contact between the droplet and the micropatch takes place, which resembles that of the smooth surface of p-Ti.

Additionally, contact angle measurements of Ag-NT-Ti were also conducted after different UV irradiation periods, revealing an enhanced hydrophilic nature of the surface (Figure 5B). Thus, the contact angle decreased, and after only 20 min of irradiation, the Ag-NT-Ti contact angle reached values below 20°, showing a superhydrophilic tendency.[63,64] It is noteworthy that this tendency occurred in samples obtained after a lower

annealing temperature compared to other Ag-containing TiO_2 films.[63]

UV irradiation is indeed applied in the cases of severely infected Ti implants. In a recent article related to infections caused by bacterial biofilms, it was reported that the yield of hydroxyl radicals generated by the combination treatment of Ag ions + UV irradiation was 10−40 times greater than that obtained with Ag application alone.[65] Furthermore, it was reported that Ti surfaces with photocatalytic hydrophilicity after UV irradiation showed a significant increase in cell attachment, spreading, and proliferation on this surface, favoring future implant attachment.[66]

3.5. Raman Analysis. Raman analysis was employed to investigate the effect of Ag patches on the microstructural properties of diverse types of nanostructured TiO_2. Characteristic bands of the six active Raman modes of the anatase crystalline phase of TiO_2 were detected on NT-Ti samples (Figure 6 and Table 1). For the Ag-NT-Ti samples, since they
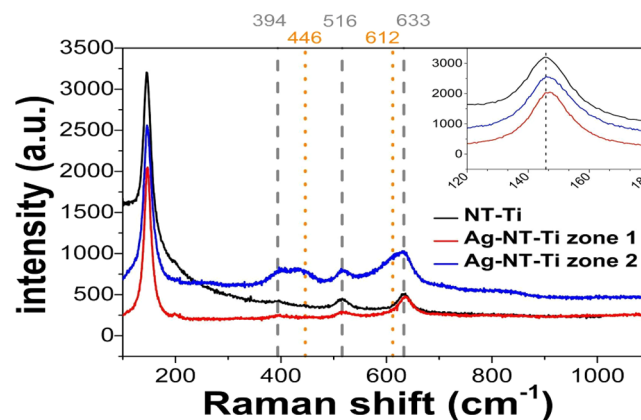

Figure 6. Raman spectra of Ag-NT-Ti (zones 1 and 2) and NT-Ti. Vertical lines indicate main rutile (orange lines) and anatase (gray lines) contributions. The inset shows the shift on the main peak of TiO_2 in the case of Ag-NT-Ti samples compared to NT-Ti.

contain surface patches of Ag, Raman spectra had to be characterized in different zones, which were selected randomly between regions that show different microscopic characteristics, showing two main spectral behaviors. The vibrational modes corresponding to the anatase were present in Ag-NT-Ti samples (represented in zone 1), but rutile vibrations (259.96, 431.26, and 629.48 cm^{-1}) were detected only in certain zones of the sample, represented in Ag-NT-Ti zone 2. Thus, the presence of

Table 1. Peak Position Values of Raman Spectra of NT-Ti and Ag-NT-Ti Samples

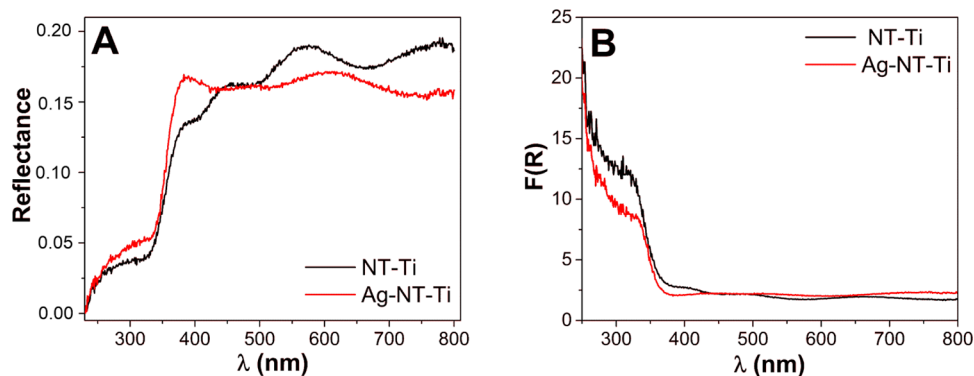| sample	position of Raman peaks (cm^{-1})[a]					
NT-Ti	144.95 (a)	199.47 (a)		394.54 (a)		516.56 (a)	633.33 (a)
Ag-NT-Ti (zone 1)	146.32 (a)	197.97 (a)		394.03 (a)		519.92 (a)	637.65 (a)
Ag-NT-Ti (zone 2)	146.31 (a)		259.96 (r)	402.43 (a)	431.26 (r)	519.92 (a)	629.48 (r)

[a](a): anatase, (r): rutile.

Figure 7. Diffuse reflectance spectra. (A) DRS spectra of NT-Ti (black) and Ag-NT-Ti (red) samples. (B) Kubelka−Munk function obtained from total reflectance measurements.
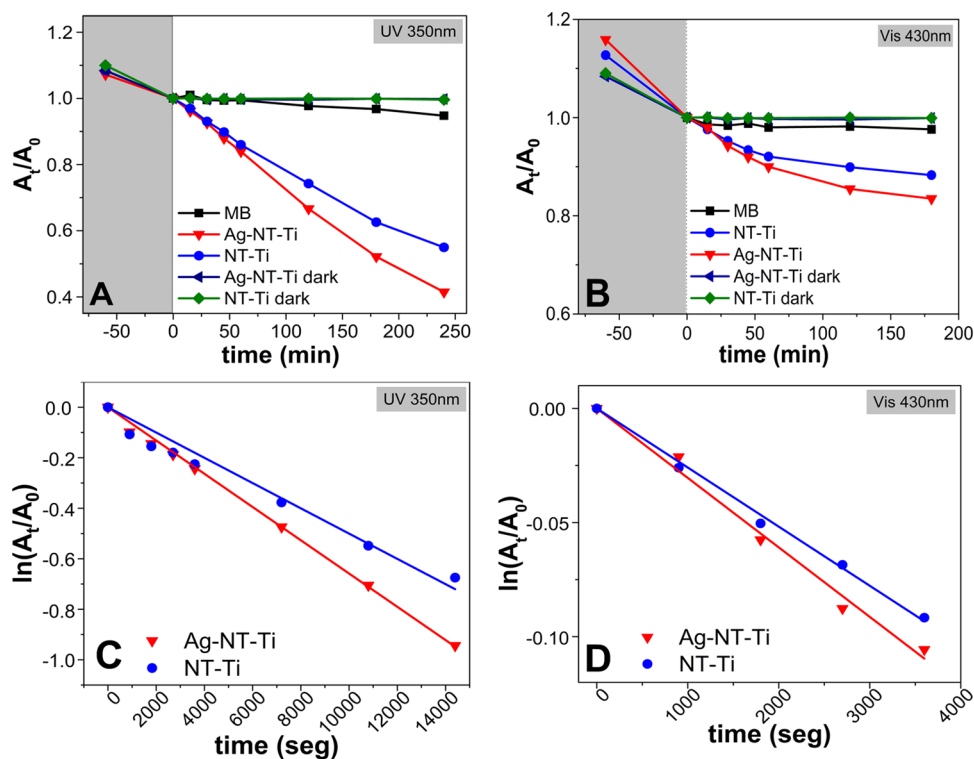

Figure 8. Photolysis assays. MB removal vs irradiation time in the presence and absence of the different samples. (A) Irradiation was performed with eight UV lamps emitting at 350 nm and (B) with LEDs of 430 nm. Gray zones in A and B represent the time before lamp ignition. Ag-NT-Ti and NT-Ti dark lines and symbols stand for MB adsorption in the materials during the time of the experiments in the absence of irradiation (blue triangles, ◀; green diamonds ♦). (C, D) Discoloration of MB vs irradiation time with NT-Ti (blue circles ●) and Ag-NT-Ti (red triangles ▼) using UV (C) and Vis irradiation (D). From the slopes of the linear fit, k_{app} was calculated.

Ag in zone 2 modifies the physicochemical properties of the TiO$_2$ nanotubes. Thus, according to Raman analysis, a nonhomogeneous anatase/rutile distribution is found in our samples that may be linked to the patched distribution of Ag on the samples.

Regarding this, Mosquera et al. reported that in the presence of metallic AgNPs, the transition temperature of anatase−rutile occurs at lower temperatures compared with bared TiO$_2$,[63] enhancing the formation of the rutile phase during the annealing step.[67] It is believed that this effect is promoted by the formation of Ag clusters, which reduces the available space to maintain relatively high volume for the anatase unit cell. On that basis, the spectra in both zones of Ag-NT-Ti samples depicted a shift in some of the main TiO$_2$ modes (Table 1), indicating that some

structural deformation happened in TiO_2 unit cells when Ag was added. Additionally, it was reported that the shift and width of the main Raman peaks of the anatase structure are strongly dependent on the presence of additional elements and on their concentration as well as the oxygen content.[68]

According to Mosquera et al.,[63] both wettability and anatase/rutile relationship are dependent on the annealing temperature and on the Ag surface content. In this regard, our results revealed the presence of rutile and the superhydrophilic tendency (after 20 min of UV irradiation) at a lower annealing temperature and higher Ag average surface content than those expected when using other Ag-containing TiO_2 films.[63]

3.6. DRS Measurements. To determine the optical properties of NT-Ti and Ag-NT-Ti materials, DRS experiments were carried out by applying the Kubelka−Munk theory (eq 2) and Tauc plot (eq 3) for the estimation of the optical band gap energy.

$$F(R) = \frac{(1 - R_\infty)^2}{2R_\infty} \tag{2}$$

$$(F(R) \cdot h\nu)^{1/\gamma} = B(h\nu - E_g) \tag{3}$$

where $F(R)$ corresponds to the Kubelka−Munk remission function obtained from the reflectance measurement; R_∞ is the reflectance of an infinitely thick specimen ($R_\infty = R_{sample}/R_{standard}$), h is the Plank constant, ν is the photon's frequency, E_g is the band gap energy, and B is a constant. The coefficient γ is related to the nature of the electron transition and is equal to 2 for the indirect transition band gap associated with Ti-derived semiconductor materials.[69]

In Figure 7A,B the corresponding DRS spectra for the samples and their $F(R)$ are shown. The bands appearing at wavelengths of less than 380 nm can be attributed to the intrinsic band gap absorption of anatase TiO_2. Absorbance at higher wavelengths, visible regions, is also noticed and they are commonly found in defected, doped, or surface-modified materials. The obtained band gap energies (Figure 4S) are 3.27 and 3.26 eV for NT-Ti and Ag-NT-Ti respectively, which are in agreement with the energies reported by other authors for TiO_2 nanotube synthesis by hydrothermal, template-assisted, and electrochemical methods.[70]

Considering that the electrochemical anodization synthesis procedure to obtain NT-Ti and Ag-NT-Ti includes the use of H_3PO_4 in aqueous solution electrolytes, P may be involved in the change of the absorbance wavelengths.[71] However, the amount of P detected by XPS is the same, within experimental error, in both NT-Ti and Ag-NT-Ti (data not shown). Contribution of surface plasmon resonance of metallic Ag electrodeposition cannot be neglected.[72]

3.7. Photocatalytic Experiments. To assess the photocatalytic activity of the NT-Ti and Ag-NT-Ti samples, the decay of MB concentration during irradiation at 350 and 430 nm was evaluated. Figure 8A,B shows the decline of MB absorption at different irradiation times for NT-Ti and Ag-NT-Ti. The MB concentration decay function can be well fitted to a pseudo-first-order rate law with an apparent first-order decaying rate constant (k_{app}). The k_{app} values were calculated from the slopes of Figure 8, which are the following: $(3.0 \pm 0.1) \times 10^{-3}$ s^{-1} and $(3.95 \pm 0.06) \times 10^{-3}$ s^{-1} for NT-Ti and Ag-NT-Ti in UV experiments (Figure 7C) and $(1.55 \pm 0.03) \times 10^{-3}$ s^{-1} and $(1.83 \pm 0.06) \times 10^{-3}$ s^{-1} for NT-Ti and Ag-NT-Ti in Vis experiments, respectively (Figure 7D).

In the absence of NT-Ti and Ag-NT-Ti, less than 5% discoloration (%D) was observed after irradiation, as expected due to the low light absorption of the dye at the irradiation wavelengths used (see black square symbols ■ in Figure 8A,B). Under UV illumination, MB %D was higher in the presence of Ag-NT-Ti (61%) compared to NT-Ti (49%). Furthermore, the photocatalytic activity under visible light irradiation was also higher for Ag-NT-Ti (16% and 12% for Ag-NT-Ti and NT-Ti, respectively). The k_{app} value of Ag-NT-Ti was ∼1.3 times higher than that for NT-Ti in both sets of experiments.

It has been reported that mixtures of anatase and rutile exhibit higher photocatalytic activity compared to the pure anatase phase.[73−75] This increased activity is attributed to the interaction between the two phases, which reduces the bulk recombination of the electron−hole pairs. Consequently, anatase−rutile mixtures, as found in Ag-NT-Ti, may contribute to the superior photocatalytic activity observed in this material.[76]

In conclusion, Ag-NT-Ti depicted better photochemical activity for the discoloration of MB than that of NT-Ti. This finding is consistent with several authors who have reported enhanced degradation of organic compounds through photocatalysis using NT-Ti after the addition of AgNPs prepared by electrochemical anodization, under both UV and visible light illumination.[67,72,77,78] Thus, the micropatches of Ag°, which promote the formation of heterojunctions on NT-Ti surfaces, improve photocatalysis.[19,79,80]

The enhancement in MB degradation achieved with Ag-NT-Ti is discussed, taking into consideration various reports[44,72,78,80−82] that propose the generation of electron−hole pairs under irradiation. Photoexcited electrons (e-CB) are transferred from TiO_2 to metallic Ag, acting as a reservoir that mitigates charge recombination. Concurrently, holes in the valence band (h+VB) react with adsorbed water, generating additional hydroxyl radicals. Additionally, electrons trapped in metallic Ag react with oxygen adsorbed on its surface, producing $O_2^{•−}$ and further OH•. These reactive oxygen species can subsequently react with the organic molecule MB, thereby enhancing the photocatalytic activity.

■ CONCLUSIONS

- An innovative method was developed to improve NT-Ti surfaces by achieving stable and active Ag^0 micropatches on TiO_2 nanotubes. The method consists of immersing the samples with NT in a AgNO$_3$ solution, followed by anodizing at +0.8 V (SCE) and annealing at 400 °C. The Ag reduction process ($Ag^{1+} + 1e^− \rightarrow Ag°$) that leads to the micropatches occurs on the surface (*in situ*).

- SEM, EDS, and XPS analysis and electrochemical assays confirmed the presence of Ag micropatches on the NT-Ti surface. Based on the Auger parameters, they can be assigned to metallic Ag.

- Raman spectra indicate that the presence of Ag on the Ag-NT-Ti surface leads to the coexistence of the rutile and anatase phases, suggesting structural changes in the original anatase phase at a low annealing temperature (400 °C).

- The WCA analysis reveals that when Ag-NT-Ti samples were subjected to UV irradiation, a significant increase in hydrophilicity was observed in samples obtained under less rigorous conditions of annealing temperature and

with a higher Ag surface content than those previously reported for TiO_2 films.

- CV electrochemical results demonstrated the excellent stability of the patches and the gradual release of Ag species into aqueous medium, with promising antimicrobial activity.

- The evaluation of photocatalytic activity at the UV range revealed that the highest MB degradation rate corresponds to Ag-NT-Ti (Ag-NT-Ti: 61% NT-Ti: 49%). Furthermore, Ag-NT-Ti also exhibited the highest photocatalytic activity when subjected to visible light irradiation (Ag-NT-Ti: 16%, NT-Ti: 12%).

Overall, the Ag-NT-Ti surfaces obtained exhibit superior properties compared to NT-Ti. The heightened photocatalytic attributes of Ag-NT-Ti surfaces, observed under both UV and visible light, suggest improved biological interactions, potentially leading to an antimicrobial effect without triggering endocytosis processes associated with AgNPs. Nevertheless, comprehensive *in vitro* and *in vivo* assays are imperative to validate these findings in biological environments.

■ ASSOCIATED CONTENT

Ⓢ Supporting Information

The Supporting Information is available free of charge at https://pubs.acs.org/doi/10.1021/acsomega.3c09687.

Chronoamperometric records of the anodization step, open-circuit potential measurements after the anodization process, determination of TiO_2 nanotube thickness by indentation, and graphical determination of E_g (PDF)

■ AUTHOR INFORMATION

Corresponding Authors

Paula Caregnato − *Instituto de Investigaciones Fisicoquímicas Teóricas y Aplicadas (INIFTA), CCT La Plata, CONICET, Facultad de Ciencias Exactas, UNLP, 1900 La Plata, Argentina;* ⓞ orcid.org/0000-0002-6780-6653; Phone: 54 221 425 7430; Email: caregnato@inifta.unlp.edu.ar; Fax: 54 221 4254642

Mónica Fernández Lorenzo de Mele − *Instituto de Investigaciones Fisicoquímicas Teóricas y Aplicadas (INIFTA), CCT La Plata, CONICET, Facultad de Ciencias Exactas, UNLP, 1900 La Plata, Argentina;* ⓞ orcid.org/0000-0002-8093-7551; Phone: 54 221 425 7430; Email: mmele@inifta.unlp.edu.ar, monica.fernandez@ing.unlp.edu.ar; Fax: 54 221 4254642

Authors

Valentina C. Cajiao Checchin − *Instituto de Investigaciones Fisicoquímicas Teóricas y Aplicadas (INIFTA), CCT La Plata, CONICET, Facultad de Ciencias Exactas, UNLP, 1900 La Plata, Argentina*

Rodolfo D. Cacciari − *Instituto de Investigaciones Fisicoquímicas Teóricas y Aplicadas (INIFTA), CCT La Plata, CONICET, Facultad de Ciencias Exactas, UNLP, 1900 La Plata, Argentina*

Aldo A. Rubert − *Instituto de Investigaciones Fisicoquímicas Teóricas y Aplicadas (INIFTA), CCT La Plata, CONICET, Facultad de Ciencias Exactas, UNLP, 1900 La Plata, Argentina;* ⓞ orcid.org/0000-0003-2224-9731

Marcela Lieblich − *Centro Nacional de Investigaciones Metalúrgicas (CENIM-CSIC), 28040 Madrid, Spain*

Natalia S. Fagali − *Instituto de Investigaciones Fisicoquímicas Teóricas y Aplicadas (INIFTA), CCT La Plata, CONICET, Facultad de Ciencias Exactas, UNLP, 1900 La Plata, Argentina*

Complete contact information is available at:
https://pubs.acs.org/10.1021/acsomega.3c09687

Notes

The authors declare no competing financial interest.

■ REFERENCES

(1) Kaur, M.; Singh, K. Review on Titanium and Titanium Based Alloys as Biomaterials for Orthopaedic Applications. *Mater. Sci. Eng., C* **2019**, *102*, 844−862.

(2) Chun, H. J.; Park, K.; Kim, C. H.; Khang, G. *Novel Biomaterials for Regenerative Medicine*; Springer, 2018.

(3) Ahn, T. K.; Lee, D. H.; Kim, T. s.; Jang, G. c.; Choi, S. J.; Oh, J. B.; Ye, G.; Lee, S. Modification of Titanium Implant and Titanium Dioxide for Bone Tissue Engineering. *Adv. Exp. Med. Biol.* **2018**, *1077*, 355−368.

(4) Mazare, A.; Totea, G.; Burnei, C.; Schmuki, P.; Demetrescu, I.; Ionita, D. Corrosion, Antibacterial Activity and Haemocompatibility of TiO2 Nanotubes as a Function of Their Annealing Temperature. *Corros. Sci.* **2016**, *103*, 215−222.

(5) Nair, M.; Elizabeth, E. Applications of Titania Nanotubes in Bone Biology. *J. Nanosci. Nanotechnol.* **2015**, *15* (2), 939−955.

(6) Mu, P.; Li, Y.; Zhang, Y.; Yang, Y.; Hu, R.; Zhao, X.; Huang, A.; Zhang, R.; Liu, X.; Huang, Q.; Lin, C. High-Throughput Screening of Rat Mesenchymal Stem Cell Behavior on Gradient TiO2 Nanotubes. *ACS Biomater. Sci. Eng.* **2018**, *4* (8), 2804−2814.

(7) Zwilling, V. Structure and physicochemistry of anodic oxide films on titanium and TA6V alloy. *Surf. Interface Anal.* **1999**, *27*, 629−637, DOI: 10.1002/(SICI)1096-9918(199907)27:7<3.0.CO;2-0.

(8) Montakhab, E.; Rashchi, F.; Sheibani, S. Modification and Photocatalytic Activity of Open Channel TiO2 Nanotubes Array Synthesized by Anodization Process. *Appl. Surf. Sci.* **2020**, *534*, No. 147581.

(9) Mohamed, H. S. H.; Rabia, M.; Zhou, X. G.; Qin, X. Sen.; Khabiri, G.; Shaban, M.; Younus, H. A.; Taha, S.; Hu, Z. Y.; Liu, J.; Li, Y.; Su, B. L. Phase-Junction Ag/TiO2 Nanocomposite as Photocathode for H2 Generation. *J. Mater. Sci. Technol.* **2021**, *83*, 179−187.

(10) Dikici, T.; Demirci, S.; Erol, M. Enhanced Photocatalytic Activity of Micro/Nano Textured TiO2 Surfaces Prepared by Sandblasting/Acid-Etching/Anodizing Process. *J. Alloys Compd.* **2017**, *694*, 246−252.

(11) Mazzarolo, A.; Lee, K.; Vicenzo, A.; Schmuki, P. Anodic TiO2 Nanotubes: Influence of Top Morphology on Their Photocatalytic Performance. *Electrochem. Commun.* **2012**, *22* (1), 162−165.

(12) Chopra, D.; Gulati, K.; Ivanovski, S. Understanding and Optimizing the Antibacterial Functions of Anodized Nano-Engineered Titanium Implants. *Acta Biomater.* **2021**, *127*, 80−101.

(13) Narendrakumar, K.; Kulkarni, M.; Addison, O.; Mazare, A.; Junkar, I.; Schmuki, P.; Sammons, R.; Iglič, A. Adherence of Oral Streptococci to Nanostructured Titanium Surfaces. *Dent. Mater.* **2015**, *31* (12), 1460−1468.

(14) Staats, K.; Pilz, M.; Sun, J.; Boiadjieva-Scherzer, T.; Kronberger, H.; Tobudic, S.; Windhager, R.; Holinka, J. Antimicrobial Potential and

Osteoblastic Cell Growth on Electrochemically Modified Titanium Surfaces with Nanotubes and Selenium or Silver Incorporation. *Sci. Rep.* **2022**, *12* (1), No. 8298, DOI: 10.1038/s41598-022-11804-6.

(15) de Avila, E. D.; Lima, B. P.; Sekiya, T.; Torii, Y.; Ogawa, T.; Shi, W.; Lux, R. Effect of UV-Photofunctionalization on Oral Bacterial Attachment and Biofilm Formation to Titanium Implant Material. *Biomaterials* **2015**, *67*, 84−92.

(16) Aita, H.; Att, W.; Ueno, T.; Yamada, M.; Hori, N.; Iwasa, F.; Tsukimura, N.; Ogawa, T. Ultraviolet Light-Mediated Photofunctionalization of Titanium to Promote Human Mesenchymal Stem Cell Migration, Attachment, Proliferation and Differentiation. *Acta Biomater.* **2009**, *5* (8), 3247−3257.

(17) Taniyama, T.; Saruta, J.; Rezaei, N. M.; Nakhaei, K.; Ghassemi, A.; Hirota, M.; Okubo, T.; Ikeda, T.; Sugita, Y.; Hasegawa, M.; Ogawa, T. UV-Photofunctionalization of Titanium Promotes Mechanical Anchorage in A Rat Osteoporosis Model. *Int. J. Mol. Sci.* **2020**, *21* (4), 1235.

(18) Peiris, S.; de Silva, H. B.; Ranasinghe, K. N.; Bandara, S. V.; Perera, I. R. Recent Development and Future Prospects of TiO2 Photocatalysis. *J. Chin. Chem. Soc.* **2021**, *68* (5), 738−769.

(19) Chakhtouna, H.; Benzeid, H.; Zari, N.; Qaiss, A. e.; Bouhfid, R. Recent Progress on Ag/TiO2 Photocatalysts: Photocatalytic and Bactericidal Behaviors. *Environ. Sci. Pollut. Res.* **2021**, *28* (33), 44638−44666, DOI: 10.1007/S11356-021-14996-Y.

(20) Liu, X.; Tian, A.; You, J.; Zhang, H.; Wu, L.; Bai, X.; Lei, Z.; Shi, X.; Xue, X.; Wang, H. Antibacterial Abilities and Biocompatibilies of Ti−Ag Alloys with Nanotubular Coatings. *Int. J. Nanomed.* **2016**, *11*, 5743−5755, DOI: 10.2147/IJN.S113674.

(21) Turu, I. C.; Bayraktar, S.; Akgul, B.; Ilhan-Sungur, E.; Abamor, E. S.; Cansever, N. Formation of TiO2 nanotubes and deposition of silver nanoparticle and reduced graphene oxide: Antibacterial and biocompatibility behaviour. *Surf. Coat. Technol.* **2023**, *470*, No. 129866, DOI: 10.1016/j.surfcoat.2023.129866.

(22) Montakhab, E.; Rashchi, F.; Sheibani, S. Enhanced photocatalytic activity of TiO2 nanotubes decorated with Ag nanoparticles by simultaneous electrochemical deposition and reduction processes. *Appl. Surf. Sci.* **2023**, *615*, No. 156332, DOI: 10.1016/j.apsusc.2023.156332.

(23) Paramasivam, I.; Macak, J. M.; Ghicov, A.; Schmuki, P. Enhanced Photochromism of Ag Loaded Self-Organized TiO2 Nanotube Layers. *Chem. Phys. Lett.* **2007**, *445* (4−6), 233−237.

(24) Paramasivam, I.; Macak, J. M.; Schmuki, P. Photocatalytic Activity of TiO2 Nanotube Layers Loaded with Ag and Au Nanoparticles. *Electrochem. Commun.* **2008**, *10* (1), 71−75.

(25) Tsai, C. Y.; Liu, C. W.; Hsi, H. C.; Lin, K. S.; Lin, Y. W.; Lai, L. C. Synthesis of Ag-Modified TiO2 Nanotube and Its Application in Photocatalytic Degradation of Dyes and Elemental Mercury. *J. Chem. Technol. Biotechnol.* **2019**, *94* (10), 3251−3262.

(26) Bilek, O.; Fialova, T.; Otahal, A.; Adam, V.; Smerkova, K.; Fohlerova, Z. Antibacterial Activity of AgNPs−TiO2 Nanotubes: Influence of Different Nanoparticle Stabilizers. *RSC Adv.* **2020**, *10* (72), 44601−44610.

(27) Pauksch, L.; Hartmann, S.; Rohnke, M.; Szalay, G.; Alt, V.; Schnettler, R.; Lips, K. S. Biocompatibility of Silver Nanoparticles and Silver Ions in Primary Human Mesenchymal Stem Cells and Osteoblasts. *Acta Biomater.* **2014**, *10* (1), 439−449.

(28) Jakubowicz, J.; Koper, J.K.; Adamek, G.; Połomska, M.; Wolak, J. Silver Nano-Trees Deposited in the Pores of Anodically Oxidized Titanium and Ti Scaffold. *Int. J. Electrochem. Sci.* **2015**, *10*, 4165−4172.

(29) Wang, R.; Xu, Y.; Wang, C.; Zhao, H.; Wang, R.; Liao, X.; Chen, L.; Chen, G. Fabrication of ITO-RGO/Ag NPs Nanocomposite by Two-Step Chronoamperometry Electrodeposition and Its Characterization as SERS Substrate. *Appl. Surf. Sci.* **2015**, *349*, 805−810.

(30) Baran, E.; YazIcI, B. Effect of Different Nano-Structured Ag Doped TiO2-NTs Fabricated by Electrodeposition on the Electrocatalytic Hydrogen Production. *Int. J. Hydrogen Energy* **2016**, *41* (4), 2498−2511.

(31) Nycz, M.; Arkusz, K.; Pijanowska, D. G. Influence of the Silver Nanoparticles (AgNPs) Formation Conditions onto Titanium Dioxide (TiO2) Nanotubes Based Electrodes on Their Impedimetric Response. *Nanomaterials* **2019**, *9* (8), 1072.

(32) Bauer, S.; Kleber, S.; Schmuki, P. TiO2 nanotubes: tailoring the geometry in H3PO4/HF electrolytes. *Electrochem. Commun.* **2006**, *8*, 1321−1325.

(33) Gravina, A. N.; Rubert, A. A.; Bertuola, M.; Fernández Lorenzo de Mele, M. Bioactivity Enhancement of Cerium-Containing Titanium Oxide Nanotubes. Relationship between Surface Reactivity and Nanostructuring Process. *Surf. Coat. Technol.* **2019**, *378*, No. 124968.

(34) Macak, J. M.; Tsuchiya, H.; Ghicov, A.; Yasuda, K.; Hahn, R.; Bauer, S.; Schmuki, P. TiO2 Nanotubes: Self-Organized Electrochemical Formation, Properties and Applications. *Curr. Opin Solid State Mater. Sci.* **2007**, *11* (1−2), 3−18.

(35) Gross, P. A.; Pronkin, S. N.; Cottineau, T.; Keller, N.; Keller, V.; Savinova, E. R. Effect of Deposition of Ag Nanoparticles on Photoelectrocatalytic Activity of Vertically Aligned TiO2 Nanotubes. *Catal. Today* **2012**, *189* (1), 93−100.

(36) Briggs, D.; Seah, M. P. Practical Surface Analysis. In *Auger and X-Ray Photoelectron Spectroscopy*; Wiley, 1990; Vol. 1.

(37) Jablonski, A.; Powell, C. J. The Electron Attenuation Length Revisited. *Surf. Sci. Rep.* **2002**, *47* (2−3), 33−91.

(38) Zhang, T.; Wang, L.; Chen, Q.; Chen, C. Cytotoxic Potential of Silver Nanoparticles. *Yonsei Med. J.* **2014**, *55* (2), 283−291.

(39) Rohde, M. M.; Snyder, C. M.; Sloop, J.; Solst, S. R.; Donati, G. L.; Spitz, D. R.; Furdui, C. M.; Singh, R. The Mechanism of Cell Death Induced by Silver Nanoparticles Is Distinct from Silver Cations. *Part. Fibre Toxicol.* **2021**, *18* (1), No. 37, DOI: 10.1186/s12989-021-00430-1.

(40) Albers, C. E.; Hofstetter, W.; Siebenrock, K. A.; Landmann, R.; Klenke, F. M. In Vitro Cytotoxicity of Silver Nanoparticles on Osteoblasts and Osteoclasts at Antibacterial Concentrations. *Nanotoxicology* **2013**, *7* (1), 30−36.

(41) Zheng, H.; Tian, Y.; Gao, Q.; Yu, Y.; Xia, X.; Feng, Z.; Dong, F.; Wu, X.; Sui, L. Hierarchical Micro-Nano Topography Promotes Cell Adhesion and Osteogenic Differentiation via Integrin A2-PI3K-AKT Signaling Axis. *Front. Bioeng. Biotechnol.* **2020**, *8*, No. 544372.

(42) Cai, S.; Wu, C.; Yang, W.; Liang, W.; Yu, H.; Liu, L. Recent Advance in Surface Modification for Regulating Cell Adhesion and Behaviors. *Nanotechnol. Rev.* **2020**, *9* (1), 971−989.

(43) Hilario, F.; Roche, V.; Nogueira, R. P.; Junior, A. M. J. Influence of Morphology and Crystalline Structure of TiO2 Nanotubes on Their Electrochemical Properties and Apatite-Forming Ability. *Electrochim. Acta* **2017**, *245*, 337−349.

(44) Yang, D.; Sun, Y.; Tong, Z.; Tian, Y.; Li, Y.; Jiang, Z. Synthesis of Ag/TiO2 Nanotube Heterojunction with Improved Visible-Light Photocatalytic Performance Inspired by Bioadhesion. *J. Phys. Chem. C* **2015**, *119* (11), 5827−5835.

(45) Xiao, Di.; Li, X.; Wang, D.; Li, Q.; Shen, K.; Wang, D. CdTe Thin Film Solar Cell with NiO as a Back Contact Buffer Layer. *Sol. Energy Mater. Sol. Cells* **2017**, *169*, 61−67.

(46) MacAk, J. M.; Sirotna, K.; Schmuki, P. Self-Organized Porous Titanium Oxide Prepared in Na2SO4/NaF Electrolytes. *Electrochim. Acta* **2005**, *50* (18), 3679−3684.

(47) Innocenti, M.; Zafferoni, C.; Lavacchi, A.; Becucci, L.; Di Benedetto, F.; Carretti, E.; Vizza, F.; Foresti, M. L. Electroactivation of Microparticles of Silver on Glassy Carbon for Oxygen Reduction and Oxidation Reactions. *J. Electrochem. Soc.* **2014**, *161* (7), D3018−D3024.

(48) Blizanac, B. B.; Ross, P. N.; Markovic, N. M. Oxygen Electroreduction on Ag(1 1 1): The PH Effect. *Electrochim. Acta* **2007**, *52* (6), 2264−2271.

(49) Blizanac, B. B.; Ross, P. N.; Marković, N. M. Oxygen Reduction on Silver Low-Index Single-Crystal Surfaces in Alkaline Solution: Rotating Ring Disk(Ag(Hkl)) Studies. *J. Phys. Chem. B* **2006**, *110* (10), 4735−4741.

(50) Bayesov, A.; Tuleshova, E.; Tukibayeva, A.; Aibolova, G.; Baineyeva, F. Electrochemical Behavior of Silver Electrode in Sulphuric Acidic Solution during Anodic Polarization. *Orient. J. Chem.* **2015**, *31* (4), 1867−1872.

(51) Brolo, A. G.; Sharma, S. D. Using Probe Beam Deflection (PBD) to Investigate the Electrochemical Oxidation of Silver in Perchlorate Media in the Presence and Absence of Chloride Ions. *Electrochim. Acta* **2003**, *48* (10), 1375−1384.

(52) Comas, C.; Huet, F.; Ngo, K.; Fregonese, M.; Idrissi, H.; Normand, B. Corrosion Propagation Monitoring Using Electrochemical Noise Measurements on Carbon Steel in Hydrogenocarbonated Solution Containing Chloride Ions. *Corros. Sci.* **2021**, *193*, No. 109885.

(53) Kakinuma, H.; Muto, I.; Oya, Y.; Momii, T.; Sugawara, Y.; Hara, N. Morphological Change and Open-circuit Potential of Single Metastable Pit on AA1050 Aluminum in NaCl Solution. *J. Electrochem. Soc.* **2021**, *168*, No. 021504, DOI: 10.1149/1945-7111/abdee9.

(54) Engelhard, M. H.; Baer, D. R.; Chen, L. X-Ray Photoelectron Spectroscopy Data from Lightly Pd Doped TiO2 Anatase Nanoparticles. *Surf. Sci. Spectra* **2020**, *27* (2), No. 024011.

(55) Jung, M.; Choi, Y. W. Localized Surface Plasmon Resonance and Structural Characteristics of Ti Nanodot Arrays Covered with an Amorphous TiO2 Native Oxide Layer. *Mater. Lett.* **2021**, *286*, No. 129223.

(56) Chae, I. S.; Hong, J.; Kang, S. W. Highly Polarized Anatase TiO2 Nanoparticles by Poly(Ethylene Phthalate). *Macromol. Res.* **2011**, *19* (9), 948−950.

(57) Russat, J. Characterization of Polyamic Acid/Polyimide Films in the Nanometric Thickness Range from Spin-Deposited Polyamic Acid. *Surf. Interface Anal.* **1988**, *11* (8), 414−420.

(58) Pertsin, A. J.; Gorelova, M. M.; Levin, V. Y.; Makarova, L. I. An XPS Study of the Surface−Bulk Compositional Differences in Siloxane-Containing Block Copolymers and Polymer Blends. *J. Appl. Polym. Sci.* **1992**, *45* (7), 1195−1202.

(59) Powell, C. J. Recommended Auger Parameters for 42 Elemental Solids. *J. Electron Spectrosc. Relat. Phenom.* **2012**, *185* (1−2), 1−3.

(60) Ferraria, A. M.; Carapeto, A. P.; Botelho Do Rego, A. M. X-Ray Photoelectron Spectroscopy: Silver Salts Revisited. *Vacuum* **2012**, *86* (12), 1988−1991.

(61) *NIST X-ray Photoelectron Spectroscopy (XPS) Database*, version 3.5. https://srdata.nist.gov/xps/ (accessed July 06, 2023).

(62) Ryan, B. J.; Poduska, K. M. Roughness effects on contact angle measurements. *Am. J. Phys.* **2008**, *76* (11), 1074−1077.

(63) Mosquera, A. A.; Albella, J. M.; Navarro, V.; Bhattacharyya, D.; Endrino, J. L. Effect of Silver on the Phase Transition and Wettability of Titanium Oxide Films. *Sci. Rep.* **2016**, *6* (1), No. 32171, DOI: 10.1038/srep32171.

(64) Wang, R.; Hashimoto, K.; Fujishima, A.; Chikuni, M.; Kojima, E.; Kitamura, A.; Shimohigoshi, M.; Watanabe, T. Light-Induced Amphiphilic Surfaces. *Nature* **1997**, *388* (6641), 431−432.

(65) Tenkumo, T.; Ishiyama, K.; Prymak, O.; Nakamura, K.; Shirato, M.; Ogawa, T.; Miyashita, M.; Takahashi, M.; Epple, M.; Kanno, T.; Sasaki, K. Bactericidal Activity and Recovery Effect of Hydroxyl Radicals Generated by Ultraviolet Irradiation and Silver Ion Application on an Infected Titanium Surface. *Sci. Rep.* **2020**, *10* (1), No. 8553, DOI: 10.1038/s41598-020-65411-4.

(66) Sawase, T.; Jimbo, R.; Baba, K.; Shibata, Y.; Ikeda, T.; Atsuta, M. Photo-Induced Hydrophilicity Enhances Initial Cell Behavior and Early Bone Apposition. *Clin. Oral Implants Res.* **2008**, *19* (5), 491−496.

(67) Viet, P. V.; Phan, B. T.; Mott, D.; Maenosono, S.; Sang, T. T.; Thi, C. M.; Hieu, L. V. Silver Nanoparticle Loaded TiO2 Nanotubes with High Photocatalytic and Antibacterial Activity Synthesized by Photoreduction Method. *J. Photochem. Photobiol., A* **2018**, *352*, 106−112, DOI: 10.1016/J.JPHOTOCHEM.2017.10.051.

(68) Mazzolini, P.; Russo, V.; Casari, C. S.; Hitosugi, T.; Nakao, S.; Hasegawa, T.; Li Bassi, A. Vibrational-Electrical Properties Relationship in Donor-Doped TiO2 by Raman Spectroscopy. *J. Phys. Chem. C* **2016**, *120* (33), 18878−18886.

(69) Makuła, P.; Pacia, M.; Macyk, W. How To Correctly Determine the Band Gap Energy of Modified Semiconductor Photocatalysts Based on UV-Vis Spectra. *J. Phys. Chem. Lett.* **2018**, *9* (23), 6814−6817.

(70) Liang, H. C.; Li, X. Z.; Nowotny, J. Photocatalytical Properties of TiO2 Nanotubes. *Solid State Phenom.* **2010**, *162*, 295−328, DOI: 10.4028/www.scientific.net/SSP.162.295.

(71) Chen, X.; Zhang, X.; Su, Y.; Lei, L. Preparation of Visible-Light Responsive P−F-Codoped TiO2 Nanotubes. *Appl. Surf. Sci.* **2008**, *254* (20), 6693−6696.

(72) Liu, X.; Liu, Z.; Lu, J.; Wu, X.; Xu, B.; Chu, W. Electrodeposition Preparation of Ag Nanoparticles Loaded TiO2 Nanotube Arrays with Enhanced Photocatalytic Performance. *Appl. Surf. Sci.* **2014**, *288*, 513−517.

(73) Feng, Y.; Rijnaarts, H. H. M.; Yntema, D.; Gong, Z.; Dionysiou, D. D.; Cao, Z.; Miao, S.; Chen, Y.; Ye, Y.; Wang, Y. Applications of Anodized TiO2 Nanotube Arrays on the Removal of Aqueous Contaminants of Emerging Concern: A Review. *Water Res.* **2020**, *186*, No. 116327.

(74) Liu, Y.; Li, J.; Zhou, B.; Chen, H.; Wang, Z.; Cai, W. A TiO2-Nanotube-Array-Based Photocatalytic Fuel Cell Using Refractory Organic Compounds as Substrates for Electricity Generation. *Chem. Commun.* **2011**, *47* (37), 10314−10316.

(75) Miyagi, T.; Kamei, M.; Mitsuhashi, T.; Ishigaki, T.; Yamazaki, A. Charge Separation at the Rutile/Anatase Interface: A Dominant Factor of Photocatalytic Activity. *Chem. Phys. Lett.* **2004**, *390* (4−6), 399−402.

(76) Pantaroto, H. N.; Ricomini-Filho, A. P.; Bertolini, M. M.; Dias da Silva, J. H.; Azevedo Neto, N. F.; Sukotjo, C.; Rangel, E. C.; Barão, V. A. R. Antibacterial Photocatalytic Activity of Different Crystalline TiO2 Phases in Oral Multispecies Biofilm. *Dent. Mater.* **2018**, *34* (7), e182−e195.

(77) Xie, K.; Sun, L.; Wang, C.; Lai, Y.; Wang, M.; Chen, H.; Lin, C. Photoelectrocatalytic Properties of Ag Nanoparticles Loaded TiO2 Nanotube Arrays Prepared by Pulse Current Deposition. *Electrochim. Acta* **2010**, *55* (24), 7211−7218.

(78) Wang, Y.; Liu, L.; Xu, L.; Meng, C.; Zhu, W. Ag/TiO2 Nanofiber Heterostructures: Highly Enhanced Photocatalysts under Visible Light. *J. Appl. Phys.* **2013**, *113* (17), No. 174311, DOI: 10.1063/1.4803844.

(79) Foster, H. A.; Ditta, I. B.; Varghese, S.; Steele, A. Photocatalytic Disinfection Using Titanium Dioxide: Spectrum and Mechanism of Antimicrobial Activity. *Appl. Microbiol. Biotechnol.* **2011**, *90* (6), 1847−1868.

(80) Harikishore, M.; Sandhyarani, M.; Venkateswarlu, K.; Nellaippan, T. A.; Rameshbabu, N. Effect of Ag Doping on Antibacterial and Photocatalytic Activity of Nanocrystalline TiO2. *Procedia Mater. Sci.* **2014**, *6*, 557−566.

(81) Kong, D.; Tan, J. Z. Y.; Yang, F.; Zeng, J.; Zhang, X. Electrodeposited Ag Nanoparticles on TiO2 Nanorods for Enhanced UV Visible Light Photoreduction CO2 to CH4. *Appl. Surf. Sci.* **2013**, *277*, 105−110.

(82) Hou, W.; Cronin, S. B. A Review of Surface Plasmon Resonance-Enhanced Photocatalysis. *Adv. Funct. Mater.* **2013**, *23* (13), 1612−1619.